Journal of Sustainable Metallurgy (2023) 9:1759–1776
https://doi.org/10.1007/s40831-023-00763-5

RESEARCH ARTICLE

A Crucial Step Toward Carbon Neutrality in Pyrometallurgical Reduction of Nickel Slag

Desmond Attah-Kyei[1] · Dmitry Sukhomlinov[1] · Mia Tiljander[2] · Lassi Klemettinen[1] · Pekka Taskinen[1] · Ari Jokilaakso[1] · Daniel Lindberg[1]

Received: 9 May 2023 / Accepted: 18 October 2023 / Published online: 8 November 2023

Abstract

This study aims at recovering valuable metals from nickel slag by employing pyrometallurgical techniques. A large amount of slag is generated during the nickel matte smelting. Nickel slag contains valuable elements such as copper, nickel, and cobalt, which can be recovered. Disposal of this slag results in loss of resources and may cause pollution of the environment. It is important to retrieve these metals for environmental and economic reasons. In this study, the slag was reacted with non-fossil reducing agents (biochar) which were produced from hydrolysis lignin and black pellet biomass by pyrolysis at 600 and 1200 °C, and with metallurgical coke for comparison. The reduction experiments were done at 1400 °C for 15, 30, and 60 min under inert gas atmosphere. The samples were quickly quenched and analyzed with Electron Probe X-ray Microanalysis. The results showed that the use of biochar resulted in faster reaction kinetics in the reduction process compared to coke. Moreover, thermodynamic modeling was also performed using Factsage to simulate equilibria with different amounts of biochar. The metal-to-slag distribution coefficient calculated from the results of thermodynamic modeling was consistent with experimental results.

Graphical Abstract

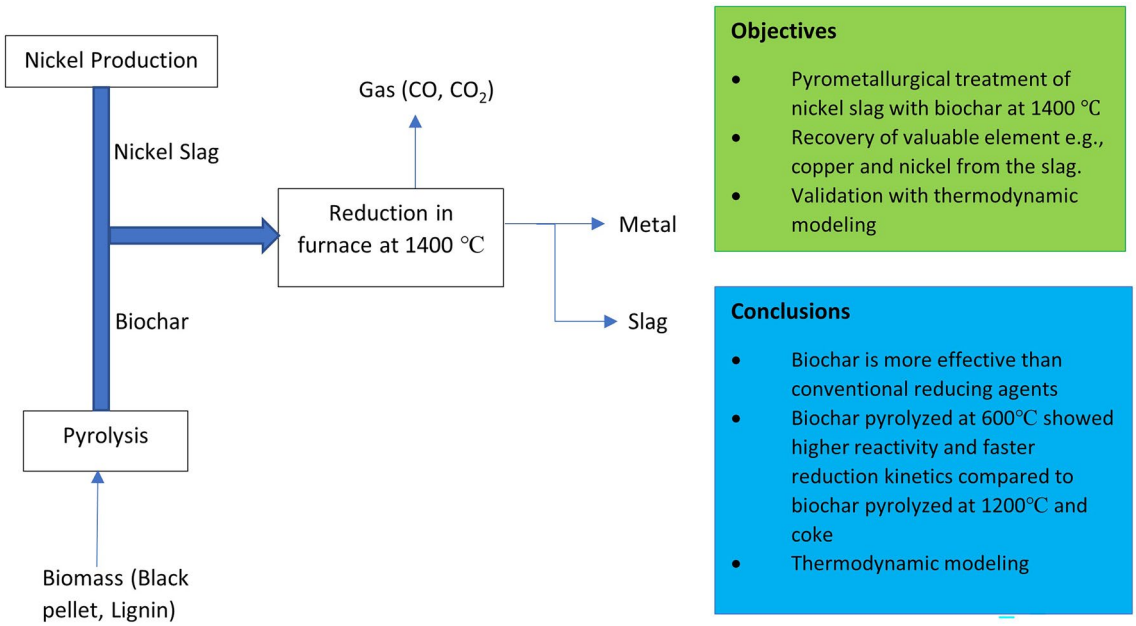

The contributing editor for this article was Hiromichi Takebe.

Extended author information available on the last page of the article

Keywords Metal recovery · Nickel slag · Biochar · Pyrometallurgical treatment · Thermodynamic modeling

Introduction

Nickel is an important non-ferrous metal which is widely used in machinery, architecture, steelmaking, military, and other fields due to its physical and chemical properties [1–3]. During the production of nickel, about 6–16 tons of nickel smelting slag is generated per ton of nickel produced [1, 4]. The slag usually contains some valuable elements such as copper, cobalt, and nickel, and these valuable metals can exist in the form of sulfides, oxides, or dissolved elements. Slags may be used for fertilizer and cement making as well as road construction, while some of them are stockpiled in heaps or controlled in landfills [4–6]. Due to its complex mineral composition, nickel slag has not been effectively utilized [7]. The negligent disposal of this waste results in environmental pollution and loss of valuable elements [4]. It is therefore important to effectively extract valuable elements from nickel slag in order to ensure environmental sustainability and efficient resource utilization, in addition to economic benefits.

Patrick et al. [6] studied the reduction behavior of nickel slag at temperatures 800–1000 °C and the effect of sodium sulfate addition. They reported XRD analysis at these temperatures indicating no reduction taking place without the additives. However, with Na_2SO_4, reduction occurs resulting in the transformation of iron-rich forsterite ($FeMgSiO_4$) phase into FeS (troillite). Sun et al. [1] investigated the recovery of valuable metals from Ni smelting slag using flotation of modified slag. The slag was modified by adding pyrite and carbon and heated to 1400 °C. They reported an increase in nickel and copper recovery by 49.6 and 43.6% relative to flotation recovery of the raw slag. Recovery of iron from nickel flash smelting (FS) slag at a nickel smelter in China, using direct reduction-magnetic separation process, has been investigated by Wang et al. [8]. In their study, calcium carbide slag was the additive and coke dust was the reductant. They aimed to optimize parameters such as reduction time, temperature, and dosage of additive for iron recovery from nickel slag. They concluded that 1287 °C, 2.8 h, and calcium carbide slag dosage of 57.19% were the optimal conditions and this resulted in iron recovery of 95.44% [8]. Zhang et al. [4] proposed nickel slag recycling using aluminum dross to investigate processes of network modification of slags and reduction at 1500 °C. They selected CaO as modifier based on thermodynamic calculations, as its use resulted in higher activity of FeO. They reported iron and copper recoveries of 94.3% and 97.8%, respectively, after aluminothermic reduction for 120 min. The metal phase revealed metallic Cu was dissolved into metallic iron forming a Fe–Cu alloy.

Dańczak et al. [9] employed anodic graphite of spent batteries as reductant in nickel slag reduction at 1350 °C. They studied the effect of different nickel slag to spent battery ratios and the phases formed at different times. It was reported that metal alloy, matte, and slag phases were formed after reduction, and they concluded that the metal/matte to slag distribution coefficient increases with an increase in the amount of spent battery. Avarmaa et al. [10], on the other hand, studied the reduction of nickel slag at 1400 °C with biochar and battery scrap mixture to recover valuable metals. They compared the results to the reduction with coke and reported that biochar enhanced reaction kinetics compared to coke and the presence of battery scrap greatly increased the distribution coefficients of valuable metals.

While nickel slag cleaning aims to recover valuable metals such as nickel, cobalt, and copper as much as possible in the metal alloy phase, it is important to minimize the iron content as it is very difficult to separate during downstream processes. Since some of the metals have similar reduction properties as iron, some losses of valuable metals are unavoidable in the slag cleaning [11]. These valuable metals are present in the slag as mechanically entrapped droplets or as chemically dissolved oxides or sulfides. To regain these elements, the mechanically entrapped metal droplets must separate, grow, and settle into the metal alloy and the dissolved oxides must be reduced with a suitable reducing agent [10].

The metallurgical industry consumes great amounts of fossil fuels such as coke, which is mainly used as fuel and reducing agent resulting in large emissions of carbon dioxide and other greenhouse gases. In recent times, the use of non-fossil reductants in metal production has gained more attention [12–14]. One such option of non-fossil reductant is biocoke or biochar obtained from pyrolyzed biomass. Since biomass absorbs CO_2 from the atmosphere during their growth, they release the absorbed CO_2 in the reduction process, thus creating a closed loop carbon cycle [15, 16]. Several research groups have investigated the use of biomass or biochar as reductant in metal production [10, 17–25].

Adrados et al. [15] compared biocokes pyrolyzed from olive and eucalyptus trees with commercial reducing agents (metallurgical coke, petroleum coke, and anthracite). They reported that based on proximate and ultimate analysis, olive and eucalyptus biocokes (bioreducers) have better quality than the usual reducing agents, since the bioreducers have lower ash and sulfur contents. Moreover, the bioreductants used have much higher specific surface

area and porosity than that of the commercial reductants, making them much more reactive. Cholico-González et al. [12] investigated the potential of using agave bagasse (biomass obtained in Mexico) as a source of reductant for magnetite concentrate. They reported that agave bagasse has a comparable reduction efficiency to fossil fuels. In their study on the effectiveness of using biomass-based reducing agent in blast furnace, Suopajärvi et al. [16] concluded that the utilization of biomass as raw material in blast furnace ironmaking can have an enormous contribution to the mitigation of CO_2 emissions in steelmaking. Moreover, Mousa et al. reported that the use of biomass as a source of energy and reducing agents provides a promising alternative solution for green steel production [26].

From an economic perspective, however, incorporating biomass reducing agents in metallurgical industries cannot currently compete with fossil reductants. On the other hand, this economic disadvantage decreases when higher carbon taxes are imposed [17, 26, 27].

The aim of this study was to ascertain the potential and effectiveness of using biochar as reducing agent to recover valuable metals like Co, Ni, and Cu from nickel smelting slag as well as to understand the effects of reaction time.

Experimental

Materials

About 1.0 g of slag was used in all experiments. The slag used was industrial (ground) nickel smelting slag provided by Boliden Harjavalta Oy (Harjavalta, Finland). X-ray fluorescence (XRF) as well as *magnetite content analyses (Satmagan) for the slag were conducted at Boliden Harjavalta Oy, see Table 1. Additionally, the slag was analyzed using XRD as shown in Fig. 1. The results showed that the slag consisted of magnetite (Fe_3O_4), olivine ($(Mg,Fe)_2SiO_4$), and fayalite (Fe_2SiO_4). Other elements shown in Table 1 were not detected due to their relatively low concentrations in the slag.

The magnetite content was initially measured to be 16.65 wt%. This initial value was used to calculate the stoichiometric amount for the reductant used. This calculation is based on the amount of carbon present in each reductant. Recalibration of Satmagan apparatus revealed a magnetite content of 22 wt% in the nickel smelting slag. Upon recalculation, the amount of carbon in the biochar employed in the reduction was 1.7 times the stoichiometric amount. Due to the difference in carbon content, the amounts of reductants used for reduction varied.

Table 1 Composition of Ni slag by XRF and its *magnetite content

Fe	Ni	Cu	Co	Cr	Zn	S	SiO_2	MgO	Al_2O_3	CaO	$*Fe_3O_4$
37	3.62	0.77	0.42	0.08	0.08	0.11	33.7	7.6	2.1	1.74	22

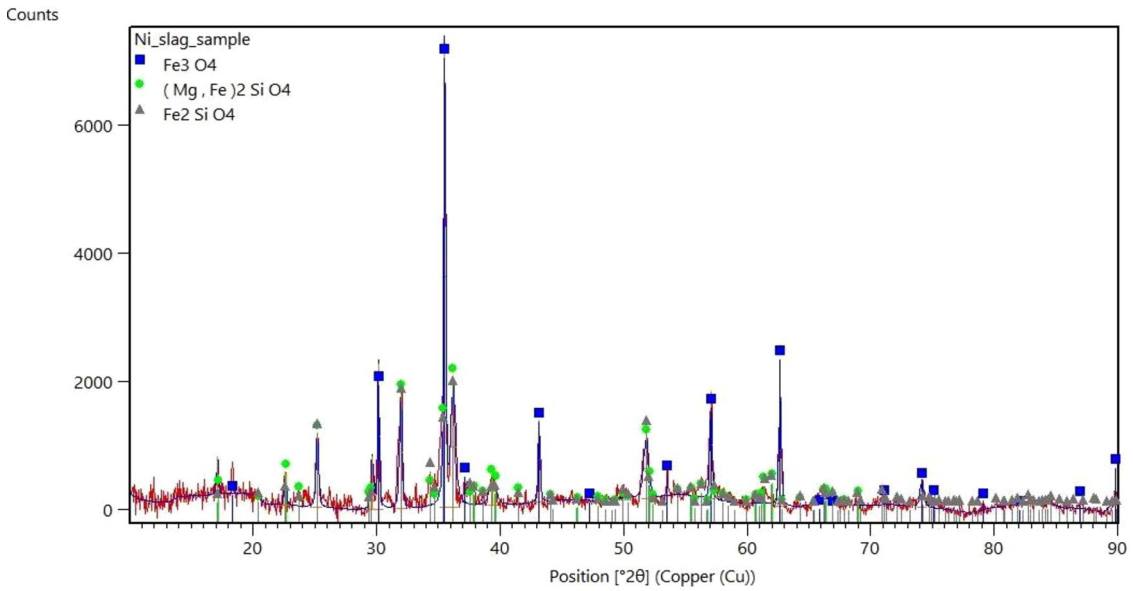

Fig. 1 XRD pattern for nickel smelting slag before reduction

Four different kinds of reductants were tested in the experiments, i.e., black pellets pyrolyzed at 600 °C (B600) and 1200 °C (B1200) and hydrolysis lignin pyrolyzed at 600 °C (L600) and 1200 °C (L1200). The samples were pyrolyzed in a chamber furnace Nabertherm HT08/18 (Nabertherm GmbH, Lilienthal, Germany) by heating from room temperature to the final temperature at 5°C/min heating rate using nitrogen as inert gas. Once the final temperature was reached, the samples were held at the final temperature for 8h. These pyrolyzed biochars were obtained from University of Oulu, Finland. The ultimate and proximate analyses of these reductants shown in Table 2 were performed at University of Oulu using Elemental Analyzer Flash 2000 CHNS-O and PerkinElmer STA 800, respectively [28]. The samples were combusted at 950 °C in determination of C, H, N, and S concentrations, while the total oxygen in the biochar was determined at 1050 °C. Ash analysis of lignin and black pellet was conducted using inductively coupled plasma-optical emission spectroscopy (ICP-OES) and is shown in Table 3.

Table 2 shows that a biomass pyrolyzed at a higher temperature has higher fixed carbon and lower volatile matter contents. In addition, the ash content of black pellet is much higher than that of lignin. The ash analysis revealed that black pellets contain relatively high concentrations of Ca, K, and Si. Most of the elements in the ash deport to the slag phase during reduction reactions. It can be seen in Table 2 that lignin has higher fixed carbon content compared to black pellet. Proximate analysis, in turn, reveals that biochar pyrolyzed at higher temperature contains higher carbon and lower hydrogen and nitrogen composition (Table 2). When biochar is employed as fuel or reducing agent in some metallurgical industries, low ash contents and high volatile matter may be advantageous [23, 29].

The stoichiometric amount of carbon required for reduction was calculated based on the composition of nickel slag after converting the metal concentrations to oxides, as shown in Eqs. (1) to (5). The stoichiometric mass of carbon to be used was calculated using Eqs. (6) to (11). The amount of reductant needed was calculated from the amount of carbon required.

$$2Cu + 0.5O_2 = Cu_2O \quad (1)$$

$$Zn + 0.5O_2 = ZnO \quad (2)$$

$$Ni + 0.5O_2 = NiO \quad (3)$$

$$Co + 0.5O_2 = CoO \quad (4)$$

$$2Cr + 1.5O_2 = Cr_2O_3 \quad (5)$$

$$Fe_3O_4 + C = 3FeO + CO \quad (6)$$

$$Cu_2O + C = 2Cu + CO \quad (7)$$

$$ZnO + C = Zn + CO \quad (8)$$

$$NiO + C = Ni + CO \quad (9)$$

$$CoO + C = Co + CO \quad (10)$$

$$Cr_2O_3 + 3C = 2Cr + 3CO \quad (11)$$

Table 2 Proximate and ultimate analyses of biochar

	Properties		L600	L1200	B600	B1200
Moisture		wt%	0.66	0.30	0.71	0.41
Ultimate analysis	C	wt%	87.90	96.73	76.62	81.21
	H	wt%	1.73	0.07	1.56	0.00
	O	wt%	8.50	2.15	7.33	5.73
	N	wt%	0.97	0.13	0.47	0.12
	S	wt%	0.00	0.00	0.00	0.00
Proximate analysis	Volatile matter	wt%	6.39	1.31	10.82	3.57
	Ash content	wt%	1.29	0.92	12.32	12.83
	Fixed carbon	wt%	91.62	97.54	76.16	83.19

Table 3 Ash analysis of biochar used for the reduction study

Element		Ca	Mg	Na	K	P	S	Fe	Al	Si	Ti	Mn	Ba	Cr	Cu	Ni	Zn
Lignin	mg/kg	290	51.0	< 10	130	74	1100	810	14	< 10	< 1.0	41	4.8	15	< 1.0	12	12
Black pellet	mg/kg	13,900	960	210	2600	560	–	680	680	7400	36	400	200	81	6	36	140

Method

The vertical-tube furnace (Fig. 2) used was Lenton LTF 16/450 (Lenton Furnaces & Ovens, Hope Valley, UK) equipped with silicon carbide heating elements, placed around alumina work tube (38 mm inner diameter and 1200 mm length) (Frialit AL23, Friatec AG, Mannheim, Germany). The temperature was monitored by a thermocouple S-type Pt/Pt-10%Rh thermocouple (Johnson-Matthey Noble Metals, UK, accuracy of ± 3 °C) and a smaller 22 mm diameter alumina tube as well as the gas inlet and a guiding tube were installed inside the work tube through a lid screw. The furnace temperature was set to 1400 °C and the temperature data during the experiments were collected with a NI LabVIEW temperature logging program. The thermocouple was connected to a Keithley 2010 DMM multimeter, and the room temperature was measured by a Pt100 resistance thermometer (SKS-Group, Vantaa, Finland, tolerance class B 1/10), connected to a Keithley 2000 DMM multimeter. The working tube was sealed from the bottom end with a rubber plug, which had a gas outlet tube that led into an exhaust line. The furnace was equipped with water cooling elements at the top and the bottom parts of the working tube. A platinum wire (diameter 0.5 mm) was inserted through the smaller diameter alumina tube for holding and lifting the samples from the cold end to the hot zone of the furnace.

The furnace was purged with argon gas (99.999 vol% purity, Woikoski Oy, Finland) with a flow rate of 300 mL/min, controlled by a rotameter (Kytölä Instruments, Jyväskylä, Finland ± 5% full scale) during the experiments. The cone-shaped silica glass Heraeus HSQ®300 crucibles (fused quartz with purity of > 99.998 wt% by Finnish Special Glass Oy, Espoo, Finland) with a diameter of 25 mm and height of 15 mm were employed for nickel slag containment.

The drop-quench technique which has been employed by several authors was used in this study. This technique was used to investigate distribution of minor elements in equilibrium [30, 31], major element phase equilibria [32, 33] as well as kinetics research [10, 34, 35].

1 g of the slag was mixed with the calculated amount of biochar. The mixture was pelletized and placed in a crucible which was in a basket-shaped sample holder made from Kanthal A-wire (diameter 0.65 mm). The basket was attached to platinum wire hanging from inside of the furnace and subsequently lifted to the lower end of the furnace before sealing the work tube with a rubber plug. At the lower

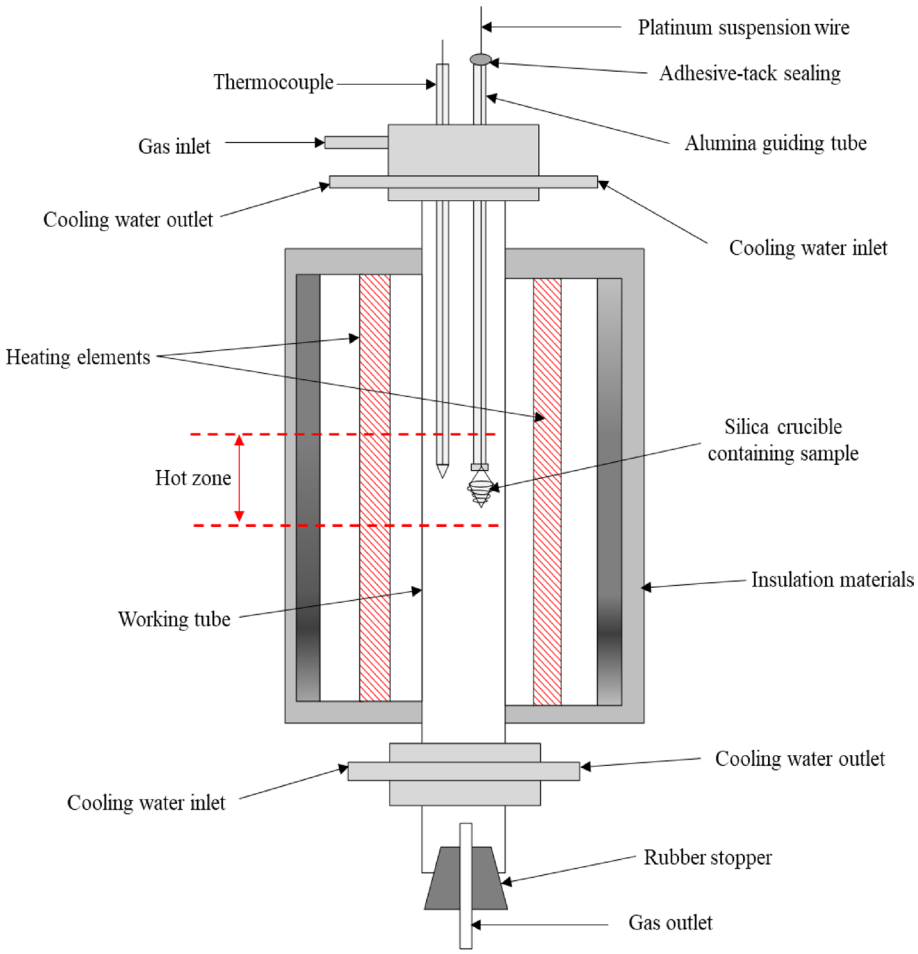

Fig. 2 Schematic of the vertical furnace used for nickel slag reduction experiments

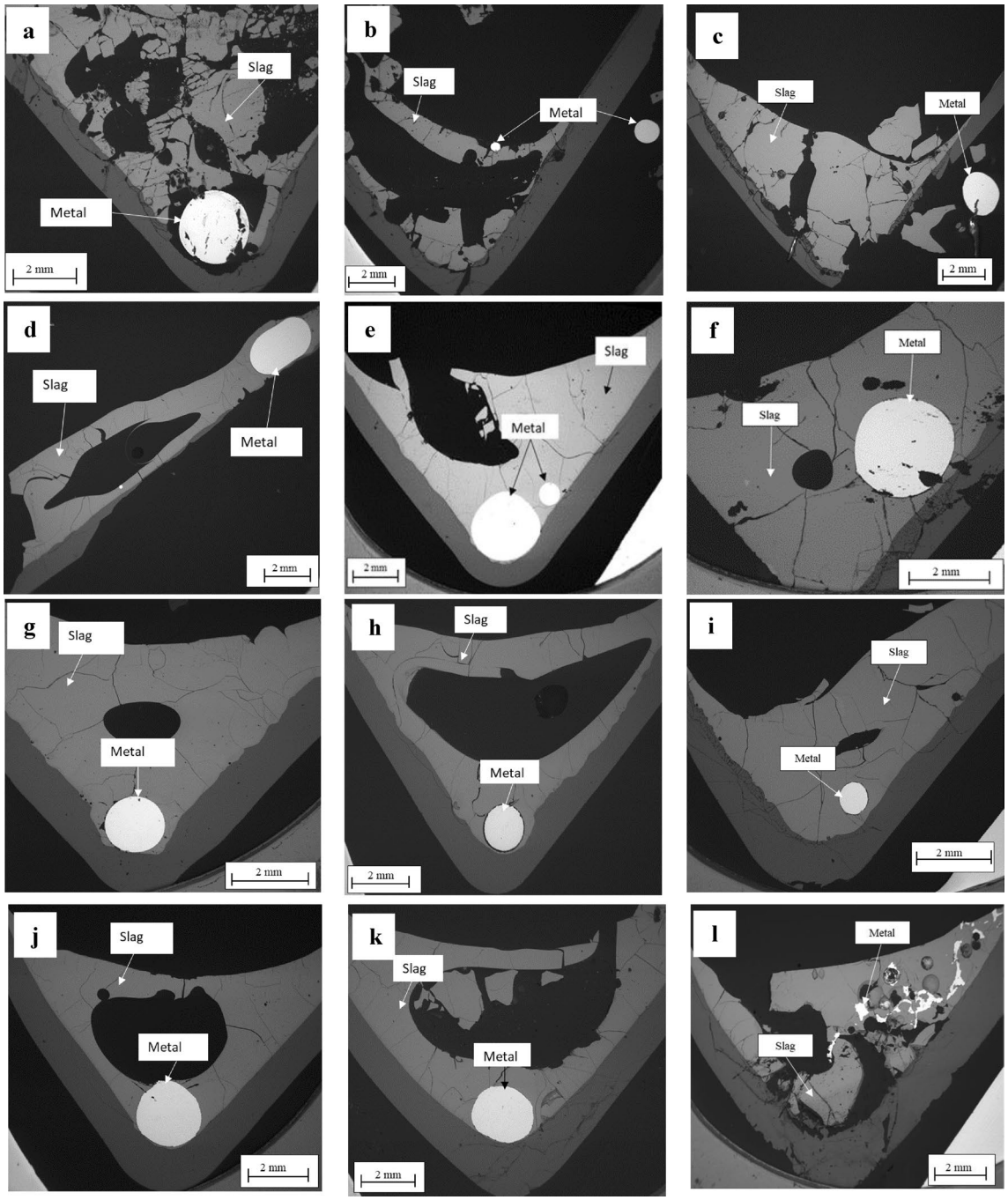

Fig. 3 SEM micrographs of sample polished sections of nickel slag reduction with **a** L1200 for 15 min, **b** L1200 for 30 min, **c** L1200 for 60 min, **d** L600 for 15 min, **e** L600 for 30 min, **f** L600 for 60 min, **g** B1200 for 15 min, **h** B1200 for 30 min, **i** B1200 for 60 min, **j** B600 for 15 min, **k** B600 for 30 min, and **l** B600 for 60 min

end of the furnace, the temperature was less than 70 °C, and therefore, no reactions were expected to take place. 300 mL/min argon gas was used to purge the furnace to create an inert atmosphere. After about 15 min, the sample was lifted to the hot zone where the reduction reactions took place. After reaching the desired reaction time, the sample was dropped into ice water by pulling the platinum wire, which caused the sample-basket assembly to detach and fall. Prior to this, the lower end of the working tube was immersed into ice water and the plug was removed thus ensuring an inert atmosphere in the furnace. Reduction experiments were carried out at 1400 °C for 15, 30, and 60 min for each of the reductants.

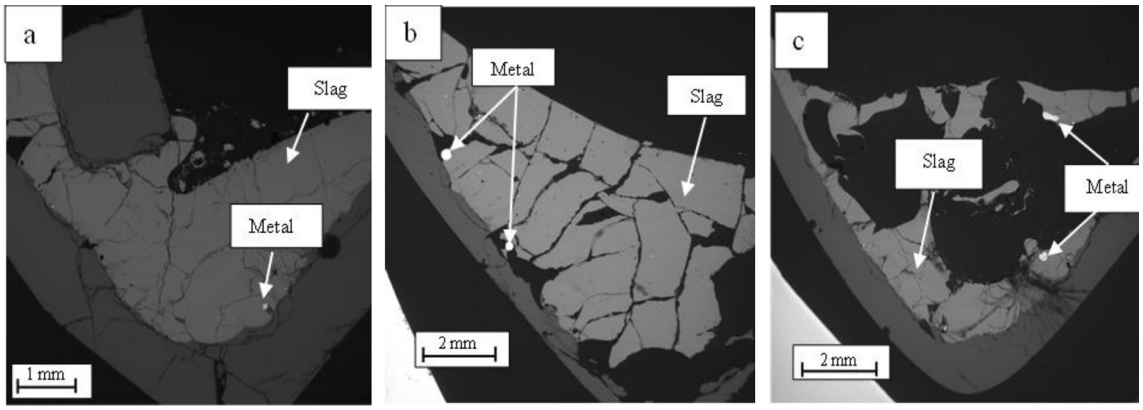

Fig. 4 SEM micrographs of sample polished sections of nickel slag with coke for **a** 15, **b** 30, and **c** 60 min

The samples were dried and cast in epoxy resin, and after curing, they were cut in half and again mounted in epoxy resin and cured. The samples were then polished, and carbon coated for scanning electron microscopy (SEM) and electron probe microanalysis (EPMA). Mira 3 Scanning Electron Microscope (Tescan, Brno, Czech Republic) equipped with an UltraDry Silicon Drift Energy Dispersive X-ray Spectrometer (EDS) supplied by Thermo Fisher Scientific (Waltham, MA, USA) was used to perform preliminary elemental analyses and microstructural imaging.

The compositions of the metal and slag phases were measured using EPMA with an SX100 (Cameca SAS, Gennevilliers, France) microprobe equipped with five wavelength dispersive spectrometers (WDS). Eight points were selected in each phase and the detection limits for the elements were determined separately in each analytical series. The acceleration voltage and beam current used were 20 kV and 30nA, respectively. A focused and defocused (2 µm or 20 µm) beam diameters were used. Standardization of the characteristic X-ray lines to be measured for the individual elements were carried out by using natural and synthetic minerals as follows: Si Kα and O Kα (quartz), Mg Kα and Ca Kα (diopside), Al Kα (almandine), Ni Kα (pure nickel), Co Kα (cobaltite), Cr Kα (chromite), Ti Kα (rutile), Fe Kα (hematite), Cu Kα (pure copper), Zn Kα (sphalerite), S Kα (sanidine), Na Kα (tugtupite), and K Kα (sanidine). Totals of the individual analysis points obtained with EPMA were typically within 100 ± 2%. The PAP-ZAF matrix correction [36] by Cameca was used for the primary WDS data.

Results and Discussion

Reduction Experiments

At the hot zone of the furnace (1400 °C), the sample melts. Metal oxides (MeO) present in the slag react with the carbon in biochar producing metal (Me) as shown in Eq. (12). Carbon monoxide produced may also take part in the reduction of metal oxides [see Eq. (13)]. As time progresses, more carbon and carbon monoxide react leading to a decrease in concentration of metals in the slag. The metal species produced from reduction of metal oxides as well as the mechanically droplets entrapped grow and form a metal alloy.

$$\mathrm{MeO(l) + C(s) = Me(l) + CO(g)} \tag{12}$$

$$\mathrm{MeO(l) + CO(g) = Me(l) + CO_2(g)} \tag{13}$$

Figure 3 shows the SEM micrographs of sample polished sections prepared from nickel slag reduction with biochar at 15, 30, and 60 min. It can be observed that a metal alloy droplet was obtained with every contacting time, which suggests that the contact between the slags and reductants was good, and the reactions proceeded rapidly. The round shaped bright regions seen in the images are the metal alloy droplets and the gray regions are the slag areas (see Fig. 3). The samples from reduction were rapidly quenched (< 3 s), resulting in homogenous slag phase with an amorphous structure. Post-quenching XRD analysis also confirmed the amorphous nature of the slag, as no crystalline peaks were detected. The average elemental concentrations of the slags and metal alloys are presented in Appendix, Tables 4, 5, and 6.

Since some of the slags were brittle because of rapid quenching, the metal droplets as well as slag pieces were sometimes detached from the rest of the sample while cutting. The dark regions (epoxy) found within the slag are attributed either to this or to gas formation within the melt.

The formed metal generally settled at the bottom of the crucible, although some smaller droplets were found in various locations inside the crucibles. Avarmaa et al. [10] observed similar microstructures and attributed the presence of the smaller droplets found at the edges of the crucibles to the surface and interfacial tensions between the phases of

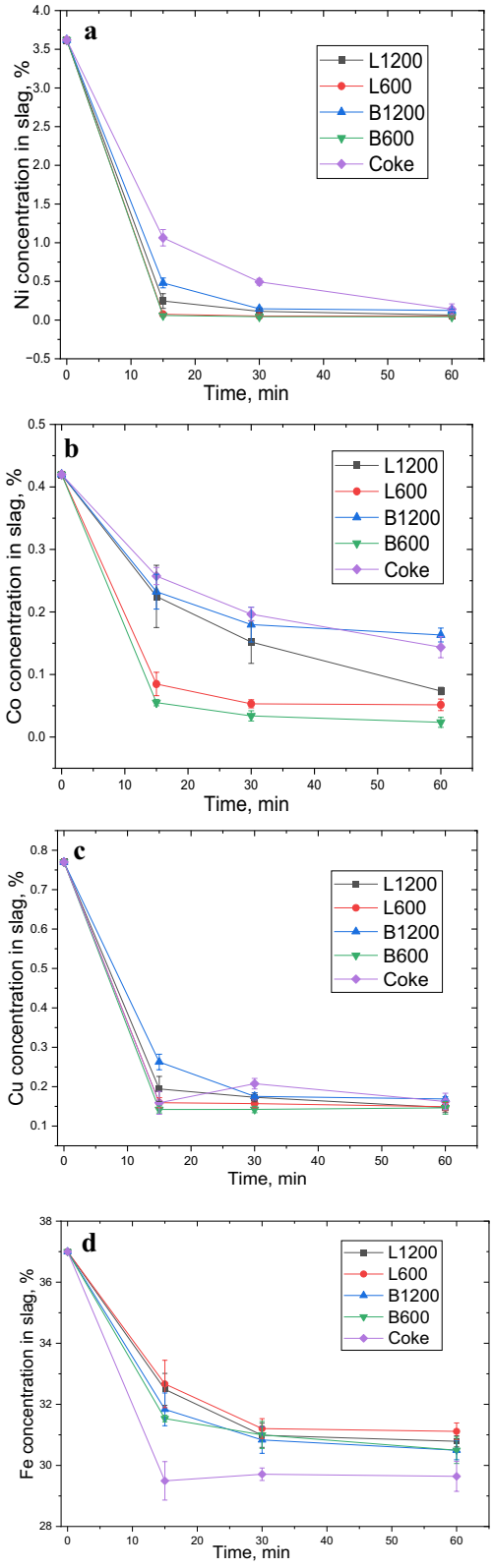

Fig. 5 Concentrations of **a** nickel, **b** cobalt, **c** copper, and **d** iron in slag as a function of time during nickel slag reduction with L1200, L600, B1200, and B600 biochar and metallurgical coke

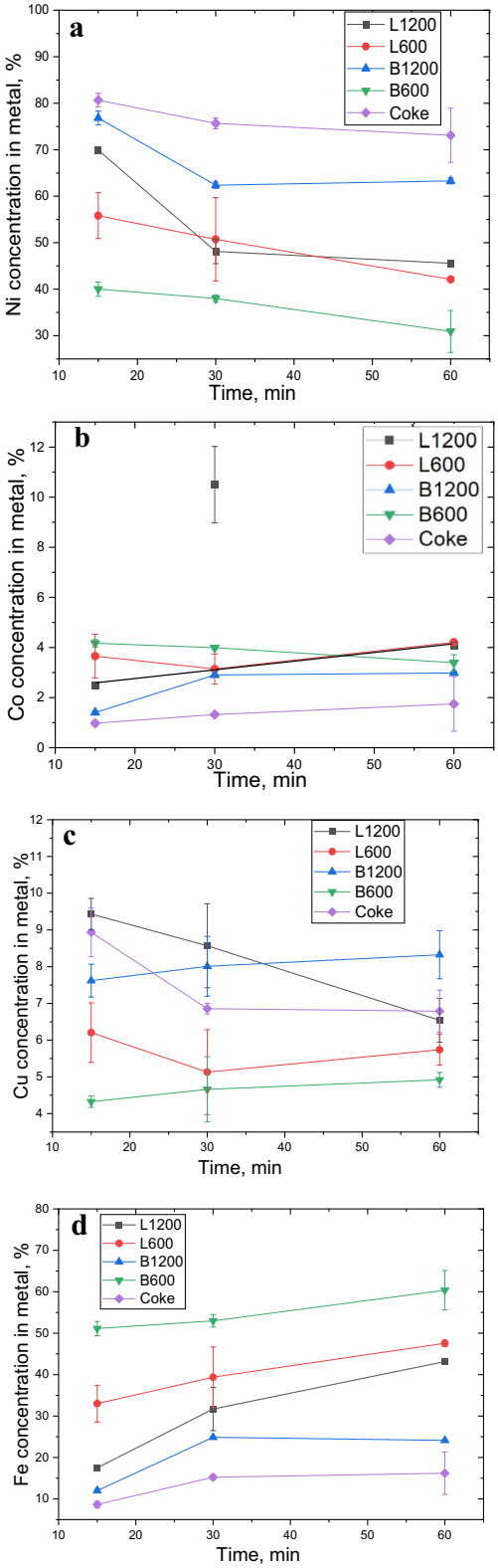

Fig. 6 Concentrations of **a** nickel, **b** cobalt, **c** copper, and **d** iron in metal alloy as a function of time during nickel slag reduction with L1200, L600, B1200, and B600 biochar and metallurgical coke

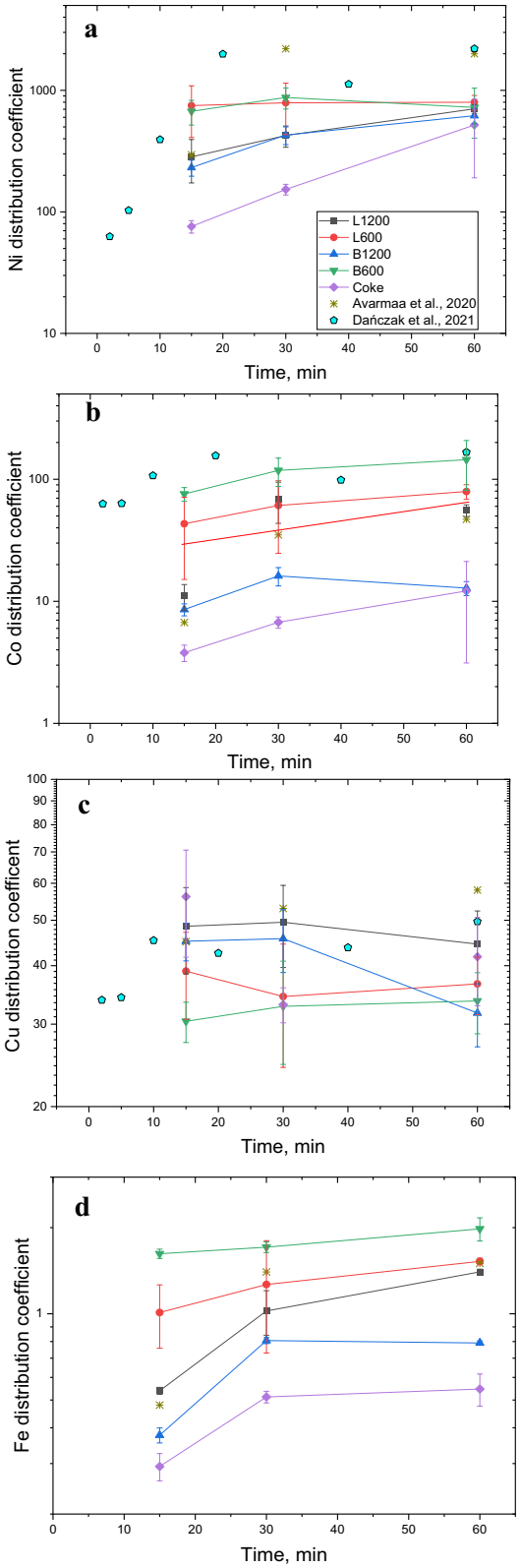

Fig. 7 Metal alloy-to-slag distribution coefficient of **a** Ni, **b** Co, **c** Cu, and **d** Fe as time progresses at 1400°C. Note the difference in the y-axis scale

the system. In some of the reduction tests, two metal droplets were found (a bigger one and a smaller one: see Fig. 3b 30 min). It is believed that the bigger droplet (> 1 mm diameter) is the first metal that was formed and the smaller one(s) is(are) later generated. Analysis of the smaller metal droplets revealed that the nickel, cobalt, and copper concentrations were higher but iron concentration was lower compared to the bigger droplet.

Nickel slag reduction was also conducted with metallurgical coke (Fig. 4) in order to compare with the results from slag reduction with biochar. It was observed that biochar is a more reactive reducing agent compared to metallurgical coke. A large metal alloy droplet (~ 2 mm diameter) was formed (Fig. 3) when the different biochars were used, but such large alloy droplets were not found in the samples reduced with coke.

Figure 5 shows the concentrations of nickel, cobalt, copper, and iron in the slag before (0 min) and after reduction (15, 30, and 60 min). This gives an indication of the amount of elements that have reduced to the metal phase or have been volatilized. It can be seen that the concentrations of nickel, cobalt, and copper in the slag decrease as reduction time increases for all the biochar types. Within the first 15 min of the reduction, nickel concentration within the slag reduced from 3.62 to 1.06 wt% when metallurgical coke was employed. Higher reduction was achieved when biochar was used, yielding nickel percentages in slag below 0.5 wt%. Biochars pyrolyzed at 600 °C (L600 and B600) showed higher reduction potentials than biochars pyrolyzed at 1200 °C. When B600 and L600 were employed as reducing agents, the nickel concentration in the slag after 15 min was 0.06 and 0.07 wt%, respectively, while those for B1200 and L1200 were 0.48 and 0.24 wt%, respectively. While biochars pyrolyzed at 1200 °C have higher carbon contents, the higher volatile matter concentrations in L600 and B600 may be indirectly responsible for their higher reactivity, i.e., showed faster reduction kinetics.

It is commonly stated that in slag cleaning processes (at 1300–1400 °C) and, e.g., in titania smelting, volatiles are not contributing the reduction processes. This means that they are not considered when calculating the stoichiometric amounts of reductant needed in the process. However, the volatile matter upon moving to the gas phase increases the surface area for sufficient slag and reductant reaction [37, 38]. Moreover, compared to the coke and biochar pyrolyzed at 1200 °C, more CO_2 is produced by biochar pyrolyzed at 600 °C which quickly reacts with solid carbon as shown in Eq. 14 (Boudouard reaction). Also, the generated CO takes part in the reduction. Since reduction with solid carbon is slower compared to CO, the higher CO present during biochar reduction increases its effectiveness as reductant compared to coke [39, 40].

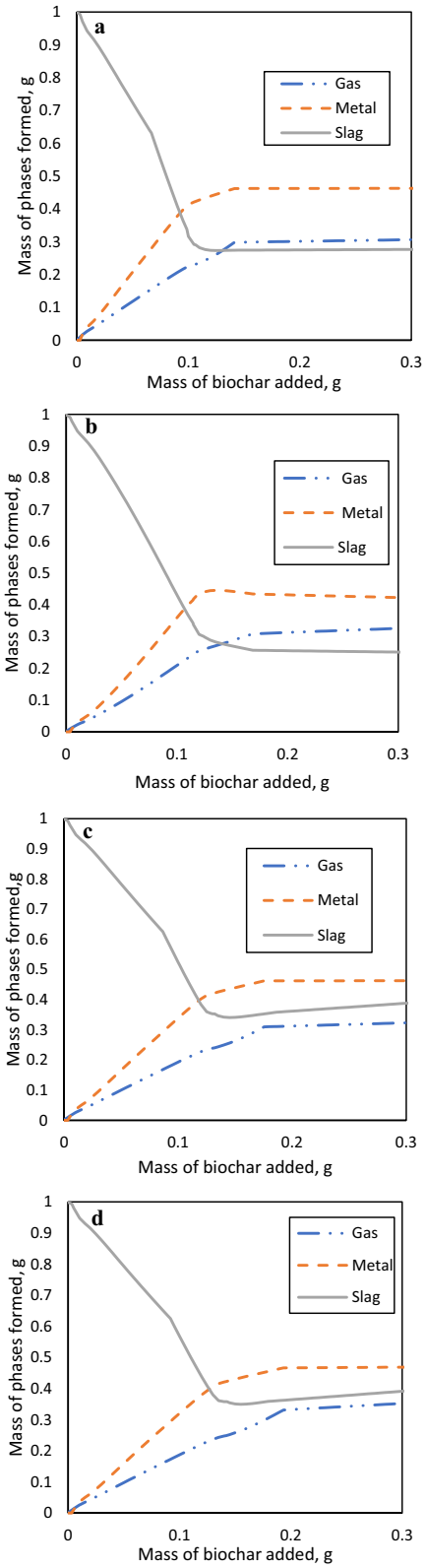

Fig. 8 Formation of gas, metal, and slag phases during nickel slag reduction with varying addition of **a** L1200, **b** L600, **c** B1200, and **d** B600 biochar to 1 g of nickel slag at 1400 °C as predicted by Factsage

$$CO_2(g) + C(s) = 2CO(g) \quad (14)$$

After 60 min reduction, the final concentrations of nickel in the slags were very close to each other with all reductants studied. Similar patterns regarding reduction kinetics of different reductants were observed for cobalt and copper as well, with the difference that the final concentration of cobalt in slag after 60 min was more than double with coke and B1200 compared to L600 and B600 reductants. Regarding iron concentration in slag, all the biochars behaved similarly; however, the use of coke resulted in the lowest iron concentrations.

The concentrations of the main elements in the metal phase (indicating the average analysis of different droplet) are shown in Fig. 6. The reduction of nickel started rapidly after reaching the experimental temperature. As time progressed, the concentration of iron increased, thus the percentage of nickel in the metal phase was reduced. In the reduction samples where more than one metal droplet was found, the results showed varying compositions, especially with nickel and iron, resulting in higher standard deviations.

Distribution Coefficients of the Elements

The distribution coefficient is a parameter that is used to estimate the progress of the reduction reaction. It gives an indication of the behavior of the various elements in the reduction study. In this work, the distribution coefficient between metal alloy and slag is used, and thus, a higher distribution coefficient indicates higher deportment to the alloy. The distribution coefficient of an element, Me, was calculated using Eq. (15) [41–43],

$$L^{m}/_{s} = \frac{\text{wt\% Me in metal}}{\text{wt\% Me in slag}}, \quad (15)$$

where m represents the metal phase and s the slag phase.

The uncertainty (ΔL) of the distribution coefficient was calculated using the relation below in Eq. (16),

$$\Delta L^{m}/_{s} = \left\{ \left[\frac{\Delta\text{Me}}{\text{wt\% Me in metal}} \right] + \left(\frac{\Delta\text{Me}}{\text{wt\% Me in slag}} \right) \right\} \times L^{m}/_{s}, \quad (16)$$

where ΔMe is the standard deviation of element Me calculated from the EPMA results.

Figure 7 shows the distribution coefficient of nickel, cobalt, copper, and iron between metal alloy and slag at 1400 °C as a function of time. The results from this work have been compared to other studies where battery scrap [9] and mixture of battery scrap and biochar [10] were used as reductants for nickel slag reduction.

The distribution coefficients of all the metals using the various reductants generally increase with time. It can be inferred from the only slightly increasing distribution

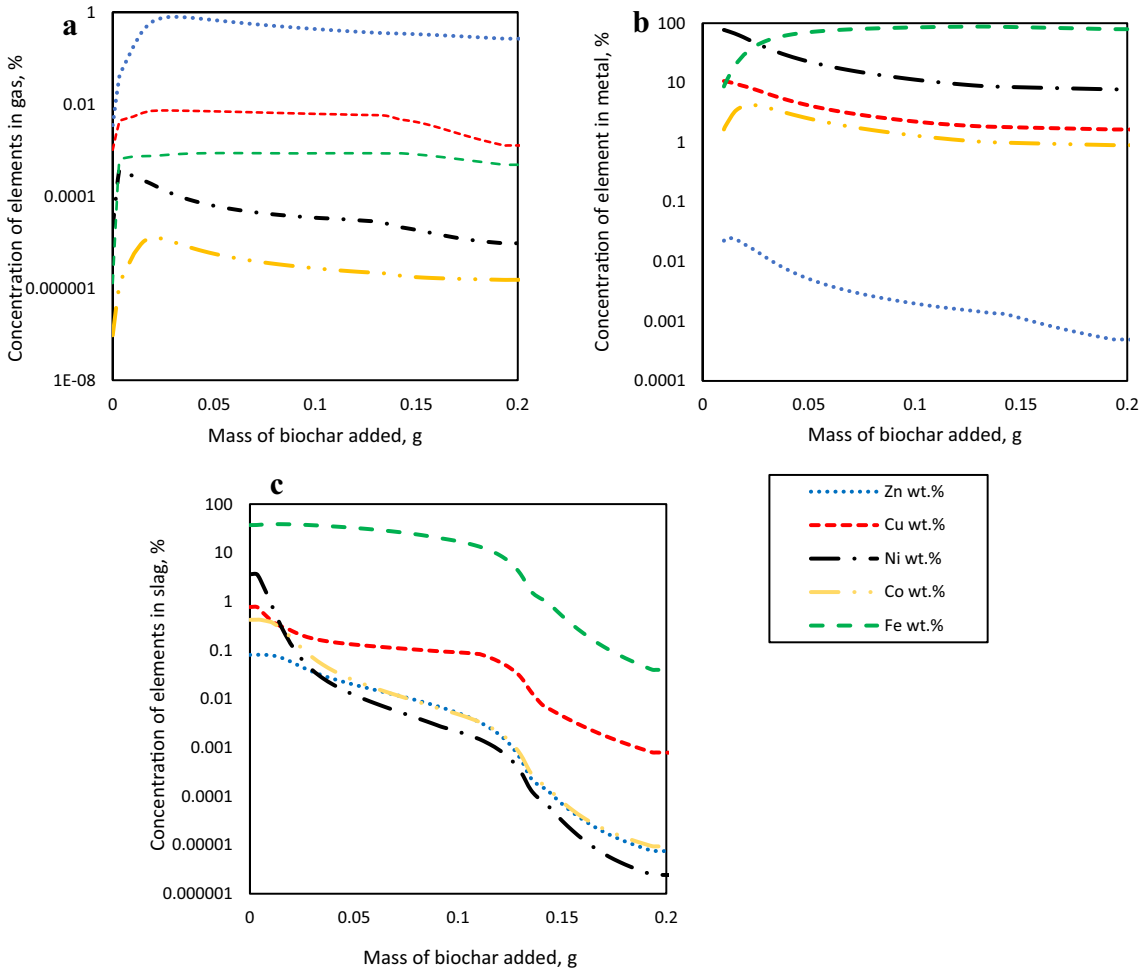

Fig. 9 Concentrations of copper, nickel, cobalt, zinc, and iron in **a** gas, **b** metal, and **c** slag phase during nickel slag reduction with varying addition of B600 biochar to 1 g of nickel slag as predicted by Factsage

coefficient values that the reduction proceeds quickly and the metal oxides are efficiently reduced to the alloy already after 15 min reduction time. The use of B600 resulted in the highest distribution coefficients for nickel, cobalt, and iron, closely followed by L600 biochar. The distribution coefficients of nickel, cobalt, and iron had the lowest values with coke reduction, although these values have the highest increase as a function of time. This is attributed to the slower reaction kinetics of coke compared to the different biochars. The distribution coefficient values for Ni and Cu are similar for coke and the biochars after 60 min of reduction. It can be inferred from Fig. 7 that in terms of the distribution coefficient values, the reductants can be ranked according to effectiveness or reactivity as B600 > L600 > L1200 > B 1200 > Coke.

Thermodynamic Modeling

Factsage thermodynamic software package, version 8.0 [44] was used in this study to investigate the effect of addition of biochar on the composition of metal and slag from nickel slag reduction in order to validate the experimental results. The composition of nickel slag, based on XRF analysis, as well as the ultimate and ash analyses of biochar were used as inputs in the software. The databases used for the calculations were custom collected based on the databases FactPS (pure substances), FToxid (optimized for oxide systems), and FSCopp (optimized for copper-containing solid and liquid alloys). The phases selected for the calculations were the spinel (solid solution phase with stoichiometry AB_2O_4, A, B = divalent and trivalent metals), slag (liquid oxide silicate phase), monoxide phase (solid solution), FCC, BCC, HCP-A3 (three solid multicomponent alloys), and liquid metal. Ideal gas and pure solids were also selected before the calculations were done at 1400 °C. The calculations with Factsage

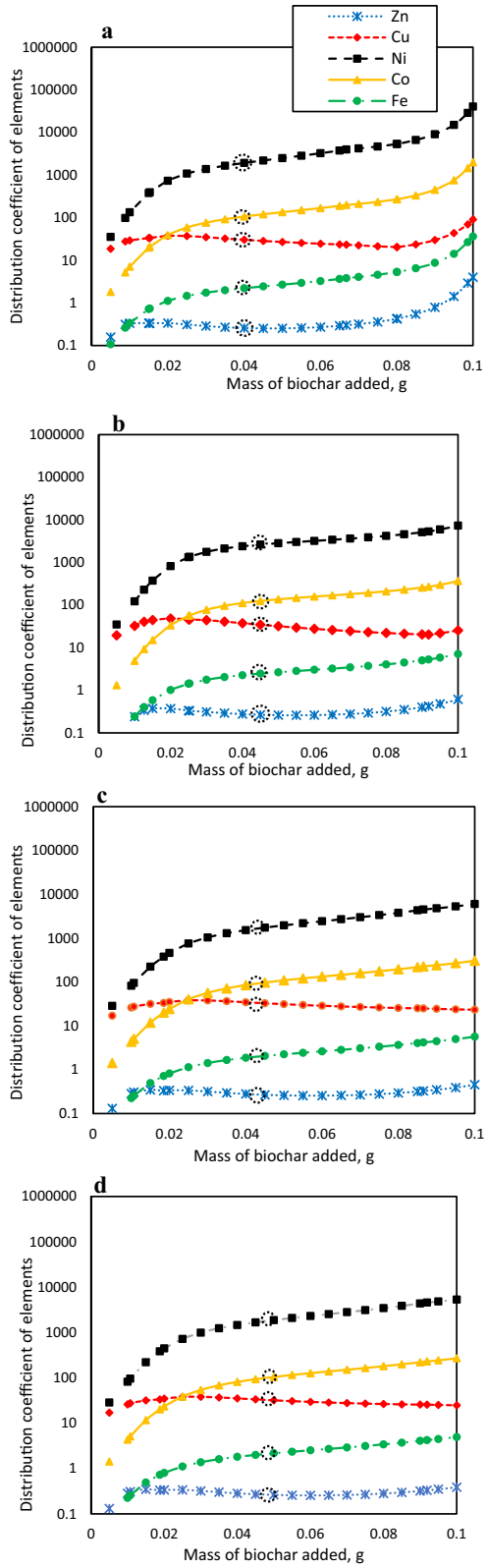

Fig. 10 Metal alloy-to-slag distribution coefficient of zinc, copper, nickel, cobalt, and iron during nickel slag reduction with varying addition of **a** L1200, **b** L600, **c** B1200, and **d** B600 biochar to 1 g of nickel slag at 1400 °C as predicted by Factsage

were performed as closed. Although argon was used to purge the furnace, it has not been included as an input in the calculations because it is assumed it did not take part in the reduction process.

Effect of Addition of Biochar

One gram of nickel slag was reacted with different masses of biochar. The phases formed during reduction, as predicted by Factsage, plotted as a function of addition of biochar are shown in Fig. 8. It is observed that as the reduction progresses, the mass of slag decreases while the masses of metal and gas increase until about 0.15 g of biochar addition. After this point, the masses of metal as well as the gas and slag remain constant. About 0.45 g of metal is formed with > 0.15 g of biochar addition. Moreover, the thermodynamic simulation reveals that relatively more gas is produced when L600 and B600 are employed as reductants compared to their respective biochars pyrolyzed at 1200 °C.

The mass percentages of some metals (Zn, Cu, Ni, Co, and Fe) that were present in the gas, metal, and slag phases are shown in Fig. 9. The results from reduction of Ni slag with B600 have been selected for plotting since the calculated results were very similar with all investigated biochars. When 0.01g of biochar is added to 1.0 g of nickel slag, at equilibrium, 80 wt% of the metal formed is nickel. This percentage continually decreases when higher amounts of biochars are added. Although the mass of nickel formed does not decrease with biochar addition, more iron is reduced, which consequently decreases the relative nickel concentration in the metal phase. In addition, the relative concentrations of copper and cobalt in the metal alloy increase to their highest values, 11% and 4% respectively, with less than 0.03 g biochar addition, after which they begin to decrease. The mass content and mass balance were not determined in the experimental section of this work, as it was not possible to separately collect all the phases from the quenched samples.

Nickel and copper have the highest concentrations of 80% and 10%, respectively, when 0.01 g of biochar is reacted with 1 g slag. The concentration of iron in the metal phase is the lowest at this addition. Since the formation of solid iron is undesired in industrial operation, it is important to recover other valuable metals like nickel and copper with low iron concentration [11].

In the slag, nickel concentration plummets to about 0.1 wt% when 0.02 g of biochar is added to a gram of slag, and it continuously decreases until the nickel oxide in slag is almost completely reduced and Ni deported to the metal phase. Cobalt followed a similar trend as nickel in the slag. However, efficient copper oxide reduction from the slag requires a higher amount of reductant compared to nickel and cobalt. According to the calculations, approximately, 0.15 g of biochar (to 1 g of slag) is enough to reduce all the

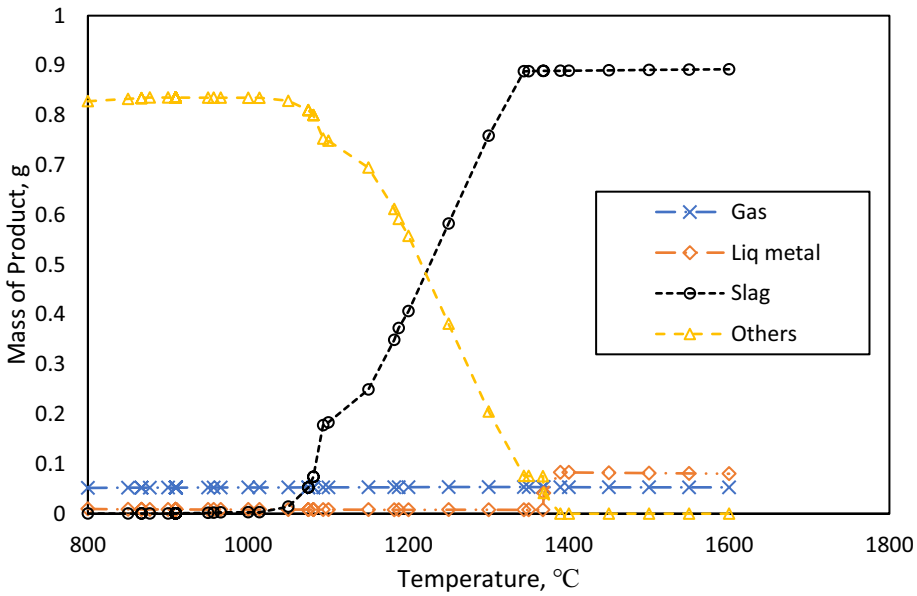

Fig. 11 Formation of gas, liquid metal, slag, and other phases (FCC, spinel, and olivine) during nickel slag reduction with B600 biochar at different temperatures as predicted by Factsage

iron oxides from the slag to metallic iron. As can be seen from Fig. 9a, zinc evaporates into the gas phase.

The metal-to-slag distribution coefficients of some elements from thermodynamic modeling of nickel slag reduction were calculated using Eq. 15 and are shown in Fig. 10. The results showed that the distribution coefficients of all the metal elements increased as a function of addition of biochar. The results of the simulations that have the same conditions as the experiments have been circled in Fig. 10.

Although the simulation yielded slightly higher distribution coefficient values, the simulation results were comparable to the experiments. In the utilization of B600 for instance, the distribution coefficient for Fe was 1.97 in the experiments and 2.17 in the simulations. This indicates that at equilibrium, more metal elements deport to the metal alloy phase as compared to the experiments probably due to kinetic restraints. It is observed that nickel distribution coefficient was the highest in each of the reduction scenarios. Iron and zinc, on the other hand, had the lowest distribution coefficients. This is consistent with the results from reduction experiments where nickel distribution coefficient was close to 1000, while that of iron was less than 10. Moreover, these results are in agreement with [10] where battery scrap was employed as reductant.

Effect of Temperature

Another thermodynamic calculation was performed by adding the stoichiometric amount of reductant to 1 g of nickel slag with temperature variations from 800 to 1600 °C. B600 has been shown as representative for the other reductants since all the thermodynamic simulations produced similar outputs. Figure 11 shows the masses of the various phases that are formed during nickel slag reduction with B600 biochar at different temperatures (800–1600 °C).

Factsage predicts the formation of gas, slag, liquid, and other phases in this temperature range. The results show that the sample melts and liquid slag starts to form at temperatures above 1150 °C. Solid phases such as spinel, olivine, and FCC are present at lower temperatures, and the sample is completely molten at temperatures above 1390 °C (Figs. 11, 12). The concentration of the main constituent of the solid phases, iron, decreases in these solid phases as iron deports to the molten slag when the temperature increases (Fig. 12c, d).

When the sample is not completely molten (< 1390 °C), nickel and cobalt are present in the FCC phase, but they completely deport to the liquid metal phase at higher temperatures. According to the calculation, nickel is expected to have a slightly higher concentration in the metal alloy phase than iron at temperatures above 1400 °C. This is due to the fact that a stoichiometric amount of reductant was used, which means that only a small fraction of the iron oxides will be reduced to metallic iron. Copper on the other hand is mainly present in the liquid metal phase even at lower temperatures. Also, zinc starts to vaporize at temperatures higher than 1000 °C and continually vaporizes with increasing temperature.

Summary and Conclusions

In this study, the use of carbon neutral biochars as reducing agents in the pyrometallurgical treatment of nickel slag was investigated at 1400 °C in order to recover valuable elements

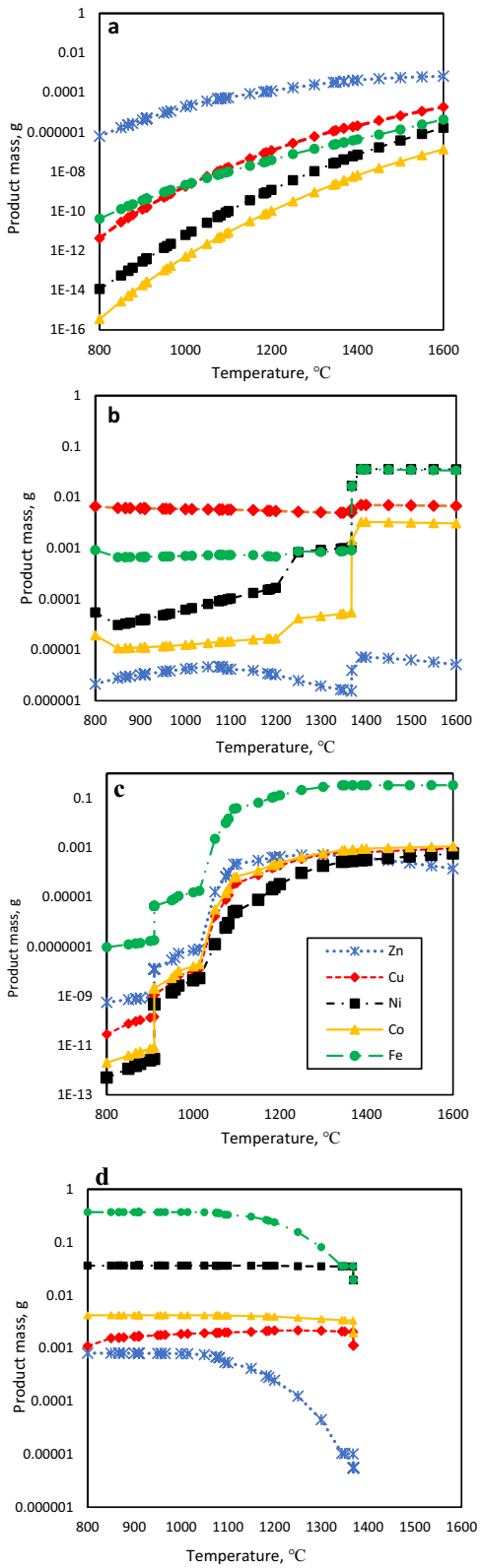

Fig. 12 Distributions of Zn, Cu, Ni, Co, and Fe in **a** gas, **b** liquid metal, **c** slag, and **d** other phases (FCC, spinel, and olivine) during nickel slag reduction with B600 biochar at different temperatures as predicted by Factsage

such as copper and nickel from the slag. Black pellet and lignin, each pyrolyzed at 600 and 1200 °C, were employed as reductants and the recoveries of nickel, copper, and cobalt were investigated and compared to the results when using fossil coke as the reductant. The biochars pyrolyzed at 1200 °C had higher fixed carbon and lower volatile matter contents compared to those pyrolyzed at 600 °C. While this may be preferred in industrial applications, the cost of energy required for pyrolyzing at higher temperatures might deter the use of biomass pyrolyzed at higher temperatures. B600 appeared to be the most efficient biochar, although it has lower carbon content compared to the other chars. The fast reaction kinetics is thought to be attributed to the relatively high content of volatiles in this biochar, leading to gas formation and thus mixing of the sample material. During the slag cleaning, biochars showed higher reactivity and faster reduction kinetics compared to coke. This, again, may be attributed to high concentration of volatile matter present. Although it is stated that at high temperatures (1300–1400 °C) volatile matter do not contribute to the reduction process, it is possible that the volatiles create pores upon moving into the gas phase, increasing thus the surface area for reaction. In addition, CO_2 generated reacts with carbon (Boudouard reaction) resulting in more CO produced which takes part in the reduction reaction. Higher distribution coefficients between metal alloy and slag were obtained for Ni, Co, and Fe using any biochar, compared to using coke.

Thermodynamic modeling was performed with FactSage© and the distribution coefficients calculated were compared to the experimental results, which were consistent with the thermodynamic modeling. In addition, thermodynamic calculations confirmed that nickel is reduced rapidly, and it deports to the metal alloy phase when enough ferric oxide has been removed from the slag. As the reduction progresses or extra reductant is available for reactions, more iron is deported to the metal phase. The calculations also revealed that Zn vaporizes into the gas phase.

The use of biochar is beneficial from an industrial point of view, as it requires a shorter reduction time and results in lower CO_2 emissions compared to coke. Issues related to low volume density, high moisture content, high transportation and storage costs, and poor grindability reported by [25] can be addressed by briquetting and pyrolysis of biomass [45] in order to facilitate the adoption of biochars in industrial applications.

Appendix

The average compositions of the slag and metal phases of the reduction products are shown in Tables 4, 5, and 6 below.

Table 4 Average phase composition obtained from EPMA after nickel slag reduction with biochar for 60 min, norm wt%

Element	L1200		L600		B1200		B600		Coke	
	Metal	Slag	Metal	Slag	Metal	Slag	Metal	Slag	Metal	Slag
O	0.34	39.09	0.31	38.83	0.39	39.22	0.34	37.83	0.89	39.46
Na	0.00	0.20	0.00	0.18	0.00	0.17	0.01	0.20	0.00	0.20
Mg	0.01	4.10	0.01	4.21	0.00	3.75	0.01	4.72	0.01	4.05
Al	0.00	0.95	0.00	0.99	0.00	0.88	0.00	1.04	0.00	1.04
Si	0.06	22.67	0.02	22.39	0.02	22.59	0.01	21.14	0.05	23.12
Mn	0.00	0.03	0.00	0.03	0.00	0.04	0.00	0.05	0.00	0.03
S	0.23	0.07	0.04	0.08	0.87	0.01	0.03	0.09	1.18	0.05
K	0.00	0.33	0.00	0.31	0.00	0.32	0.00	0.39	0.01	0.34
Ca	0.00	1.11	0.00	1.12	0.00	1.15	0.00	1.36	0.00	1.12
Ti	0.00	0.28	0.00	0.29	0.00	0.25	0.00	0.30	0.01	0.28
Cr	0.00	0.07	0.00	0.08	0.00	0.07	0.00	0.08	0.00	0.07
Fe	43.15	30.80	47.57	31.21	24.13	30.50	60.37	32.55	16.20	29.64
Co	4.09	0.08	4.21	0.05	2.98	0.25	3.39	0.02	1.75	0.16
Ni	45.58	0.08	42.11	0.05	63.28	0.51	30.92	0.04	73.10	0.26
Cu	6.54	0.15	5.74	0.16	8.32	0.28	4.92	0.15	6.79	0.17
Zn	0.00	0.00	0.00	0.01	0.00	0.01	0.00	0.02	0.00	0.01

Table 5 Average phase composition obtained from EPMA after nickel slag reduction with biochar for 30 min, norm wt%

Element	L1200		L600		B1200		B600		Coke	
	Metal	Slag	Metal	Slag	Metal	Slag	Metal	Slag	Metal	Slag
O	0.40	38.96	0.37	39.27	0.40	39.76	0.28	39.62	0.74	39.58
Na	0.00	0.18	0.00	0.18	0.00	0.16	0.00	0.20	0.00	0.18
Mg	0.01	3.96	0.00	4.21	0.00	3.86	0.00	4.33	0.01	3.82
Al	0.00	0.93	0.01	1.02	0.01	0.93	0.00	1.01	0.00	0.96
Si	0.05	22.72	0.10	22.01	0.02	21.99	0.02	21.45	0.02	23.08
Mn	0.00	0.03	0.00	0.03	0.00	0.04	0.00	0.05	0.00	0.03
S	0.64	0.06	1.12	0.06	1.42	0.05	0.06	0.08	0.14	0.04
K	0.00	0.32	0.00	0.32	0.00	0.31	0.00	0.35	0.01	0.31
Ca	0.00	1.06	0.00	1.14	0.00	1.23	0.00	1.31	0.00	1.04
Ti	0.00	0.27	0.00	0.29	0.00	0.26	0.01	0.30	0.00	0.26
Cr	0.00	0.07	0.00	0.08	0.00	0.07	0.00	0.08	0.00	0.07
Fe	31.70	30.99	39.37	31.11	24.87	30.83	52.99	31.00	15.23	29.71
Co	10.49	0.15	3.14	0.05	2.90	0.18	3.99	0.03	1.32	0.20
Ni	48.12	0.11	50.74	0.06	62.37	0.15	37.99	0.04	75.67	0.49
Cu	8.57	0.17	5.13	0.15	8.01	0.18	4.66	0.14	6.86	0.21
Zn	0.00	0.01	0.00	0.01	0.00	0.01	0.00	0.01	0.00	0.01

Table 6 Average phase composition obtained from EPMA after nickel slag reduction with biochar for 15 min, norm wt%

Element	L1200		L600		B1200		B600		Coke	
	Metal	Slag	Metal	Slag	Metal	Slag	Metal	Slag	Metal	Slag
O	0.52	38.46	0.47	38.61	0.34	39.03	0.30	39.23	0.68	39.61
Na	0.00	0.19	0.00	0.19	0.00	0.20	0.00	0.18	0.00	0.18
Mg	0.00	4.12	0.01	4.11	0.02	4.04	0.00	4.31	0.01	3.58
Al	0.00	0.97	0.00	0.97	0.00	0.95	0.01	1.01	0.00	0.95
Si	0.03	21.26	0.06	21.26	0.03	21.39	0.03	21.32	0.03	23.07
Mn	0.00	0.04	0.00	0.04	0.00	0.04	0.00	0.04	0.00	0.03
S	0.09	0.06	0.76	0.07	1.77	0.07	0.03	0.06	0.06	0.02
K	0.00	0.31	0.00	0.31	0.00	0.35	0.00	0.35	0.00	0.29
Ca	0.00	1.10	0.00	1.11	0.00	1.26	0.00	1.32	0.00	0.98
Ti	0.00	0.27	0.00	0.28	0.00	0.27	0.00	0.28	0.00	0.24
Cr	0.00	0.07	0.00	0.07	0.00	0.07	0.00	0.08	0.00	0.06
Fe	17.50	32.49	33.01	32.67	12.00	31.84	51.12	31.53	8.65	29.50
Co	2.48	0.21	3.66	0.08	1.40	0.17	4.17	0.06	0.98	0.26
Ni	69.93	0.23	55.82	0.07	76.82	0.13	40.01	0.06	80.65	1.06
Cu	9.43	0.19	6.21	0.16	7.62	0.17	4.32	0.14	8.94	0.16
Zn	0.00	0.03	0.00	0.01	0.00	0.02	0.00	0.01	0.00	0.01

Acknowledgements This study received financial support from Aalto University, School of Chemical Engineering TOCANEM Project (Business Finland Grant 2118452), BOLIDEN Harjavalta Oy for providing the nickel slag; University of Oulu for preparing and providing the biochars. The utilization of the Academy of Finland's RawMatTERS Finland Infrastructure (RAMI) based at Aalto University, GTK, and VTT in Espoo is appreciated

Funding Open Access funding provided by Aalto University.

Declarations

Conflict of interest The authors declare that they have no conflict of interest.

References

1. Sun W, Li X, Liu R, Zhai Q, Li J (2021) Recovery of valuable metals from nickel smelting slag based on reduction and sulfurization modification. Minerals 11:1–14. https://doi.org/10.3390/min11091022
2. Marenych O, Kostryzhev A (2020) Strengthening mechanisms in alloys: a review. Metals (Basel) 10:1–18. https://doi.org/10.1007/BF02842915
3. Mei X, Cheng H, Xu C, Li G, Lu X, Xu Q (2019) Mechanism of the chlorination roasting of nickel sulphide concentrate with ammonium chloride, 10th edn. Springer, Cham
4. Zhang G, Wang N, Chen M, Cheng Y (2020) Recycling nickel slag by aluminum dross: iron-extraction and secondary slag stabilization. ISIJ Int 60:602–609. https://doi.org/10.2355/isijinternational.ISIJINT-2019-173
5. Arnout L, Beersaerts G, Liard M, Lootens D, Pontikes Y (2021) Valorising slags from non-ferrous metallurgy into hybrid cementitious binders: mix design and performance. Waste Biomass Valoriz 12:4679–4694. https://doi.org/10.1007/s12649-020-01322-9
6. Patrick J, Prasetyo AB, Munir B, Maksum A, Soedarsono JW (2018) The effect of addition of sodium sulphate (Na_2SO_4) to nickel slag pyrometallurgical process with temperature and additives ratio as variables. E3S Web Conf 67:1–8. https://doi.org/10.1051/e3sconf/20186703053
7. Shi R, Cui Y, Zhao J, Li X, Zou C, Yu Y (2021) Direct reduction and extraction of iron from nickel smelting slag coupling of preparation of cementing materials using gangue composition. Croat Chem Acta 60:23–26
8. Wang S, Wang C, Wang Q, Ni W, Li K (2017) Optimization and microstructure study of the reduction of nickel smelting slag mixed with calcium carbide slag and coke dust for recovering iron. Chem Eng Trans 62:55–60. https://doi.org/10.3303/CET1762010
9. Dańczak A, Ruismäki R, Rinne T, Klemettinen L, O'brien H, Taskinen P, Jokilaakso A, Serna-guerrero R (2021) Worth from waste: utilizing a graphite-rich fraction from spent lithium-ion batteries as alternative reductant in nickel slag cleaning. Minerals. https://doi.org/10.3390/min11070784
10. Avarmaa K, Järvenpää M, Klemettinen L, Marjakoski M, Taskinen P, Lindberg D, Jokilaakso A (2020) Battery scrap and biochar utilization for improved metal recoveries in nickel slag cleaning conditions. Batteries 6:1–21. https://doi.org/10.3390/batteries6040058

11. Jones RT, Denton GM, Reynolds QG, Parker JAL, Van Tonder GJJ (2002) Recovery of cobalt from slag in a DC arc furnace at Chambishi, Zambia. J S Afr Inst Min Metall 102:5–9
12. Cholico-González D, Lara NO, Miranda MAS, Estrella RM, García RE, Patiño CAL (2021) Efficient metallization of magnetite concentrate by reduction with agave bagasse as a source of reducing agents. Int J Miner Metall Mater 28:603–611. https://doi.org/10.1007/s12613-020-2079-z
13. Guo D, Li Y, Cui B, Chen Z, Luo S, Xiao B, Zhu H, Hu M (2017) Direct reduction of iron ore/biomass composite pellets using simulated biomass-derived syngas: experimental analysis and kinetic modelling. Chem Eng J 327:822–830. https://doi.org/10.1016/j.cej.2017.06.118
14. Guo D, Zhu L, Guo S, Cui B, Luo S, Laghari M, Chen Z, Ma C, Zhou Y, Chen J, Xiao B, Hu M, Luo S (2016) Direct reduction of oxidized iron ore pellets using biomass syngas as the reducer. Fuel Process Technol 148:276–281. https://doi.org/10.1016/j.fuproc.2016.03.009
15. Adrados A, De Marco I, López-Urionabarrenechea A, Solar J, Caballero BM, Gastelu N (2016) Biomass pyrolysis solids as reducing agents: comparison with commercial reducing agents. Materials (Basel). https://doi.org/10.3390/ma9010003
16. Suopajärvi H, Pongrácz E, Fabritius T (2013) The potential of using biomass-based reducing agents in the blast furnace: a review of thermochemical conversion technologies and assessments related to sustainability. Renew Sustain Energy Rev 25:511–528. https://doi.org/10.1016/j.rser.2013.05.005
17. Demey H, Rodriguez-Alonso E, Lacombe E, Grateau M, Jaricot N, Chatroux A, Thiery S, Marchand M, Melkior T (2021) Upscaling severe torrefaction of agricultural residues to produce sustainable reducing agents for non-ferrous metallurgy. Metals (Basel). https://doi.org/10.3390/met11121905
18. Holland K, Eriç RH, Taskinen P, Jokilaakso A (2019) Upgrading copper slag cleaning tailings for re-use. Miner Eng 133:35–42. https://doi.org/10.1016/j.mineng.2018.12.026
19. Koskela A, Suopajärvi H, Mattila O, Uusitalo J, Fabritius T (2019) Lignin from bioethanol production as a part of a raw material blend of a metallurgical coke. Energies. https://doi.org/10.3390/en12081533
20. Srivastava U, Kawatra SK, Eisele TC (2013) Production of pig iron by utilizing biomass as a reducing agent. Int J Miner Process 119:51–57. https://doi.org/10.1016/j.minpro.2012.12.008
21. Wang C, Larsson M, Lövgren J, Nilsson L, Mellin P, Yang W, Salman H, Hultgren A (2014) Injection of solid biomass products into the blast furnace and its potential effects on an integrated steel plant. Energy Procedia 61:2184–2187. https://doi.org/10.1016/j.egypro.2014.12.105
22. Wei R, Kog L, Cang D, Li J, Li X, Xu CC (2017) Current status and potential of biomass utilization in ferrous metallurgical industry. Renew Sustain Energy Rev 68:511–524. https://doi.org/10.1016/j.rser.2016.10.013
23. Wiklund CM, Helle M, Kohl T, Järvinen M, Saxén H (2017) Feasibility study of woody-biomass use in a steel plant through process integration. J Clean Prod 142:4127–4141. https://doi.org/10.1016/j.jclepro.2016.09.210
24. Ye L, Peng Z, Wang L, Anzulevich A, Bychkov I, Kalganov D, Tang H, Rao M, Li G, Jiang T (2019) Use of biochar for sustainable ferrous metallurgy. J Miner Met Mater Soc 71:3931–3940. https://doi.org/10.1007/s11837-019-03766-4
25. Zhang J, Fu H, Liu Y, Dang H, Ye L, Conejio AN, Xu R (2022) Review on biomass metallurgy: pretreatment technology, metallurgical mechanism and process design. Int J Miner Metall Mater 29:1133–1149. https://doi.org/10.1007/s12613-022-2501-9
26. Mousa E, Wang C, Riesbeck J, Larsson M (2016) Biomass applications in iron and steel industry: an overview of challenges and opportunities. Renew Sustain Energy Rev 65:1247–1266. https://doi.org/10.1016/j.rser.2016.07.061
27. Suopajärvi H, Pongrácz E, Fabritius T (2014) Bioreducer use in Finnish blast furnace ironmaking—analysis of CO_2 emission reduction potential and mitigation cost. Appl Energy 124:82–93. https://doi.org/10.1016/j.apenergy.2014.03.008
28. Cassel B, Menard K, Earnest PC (2012) APP proximate analysis coal coke. Therm Anal 452:1–4
29. Saidur R, Abdelaziz EA, Demirbas A, Hossain MS, Mekhilef S (2011) A review on biomass as a fuel for boilers. Renew Sustain Energy Rev 15:2262–2289. https://doi.org/10.1016/j.rser.2011.02.015
30. Avarmaa K, O'Brien H, Johto H, Taskinen P (2015) Equilibrium distribution of precious metals between slag and copper matte at 1250–1350 °C. J Sustain Metall 1:216–228. https://doi.org/10.1007/s40831-015-0020-x
31. Shishin D, Hidayat T, Chen J, Hayes PC, Jak E (2019) Experimental investigation and thermodynamic modeling of the distributions of Ag and Au between slag, matte, and metal in the Cu–Fe–O–S–Si system. J Sustain Metall 5:240–249. https://doi.org/10.1007/s40831-019-00218-w
32. Hamuyuni J, Hellstén N, Akdogan G, Taskinen P (2015) The liquidus in Cu-O-CaO system at metallic copper saturation up to 1698 K. J Am Ceram Soc 98:320–323. https://doi.org/10.1111/jace.13282
33. Jak E, Zhao B, Liu N, Hayes PC (1999) Experimental study of phase equilibria in the system. Metall Mater Trans B 30B:21–27
34. Klemettinen L, Aromaa R, Dańczak A, O'Brien H, Taskinen P, Jokilaakso A (2020) Distribution kinetics of rare earth elements in copper smelting. Sustainability 12:1–17. https://doi.org/10.3390/SU12010208
35. Wan X, Shen L, Jokilaakso A, Eriç H, Taskinen P (2021) Experimental approach to matte-slag reactions in the flash smelting process. Miner Process Extr Metall Rev 42:231–241. https://doi.org/10.1080/08827508.2020.1737801
36. Pouchou J, Pichoir L (1986) Basic expression of "PAP" computation for quantitative EPMA. In: Proceedings of the 11th international congress on X-ray optics and microanalysis (ICXOM), London, ON, Canada, pp 249–256
37. Lotfian S, Ahmed H, El-Geassy AHA, Samuelsson C (2017) Alternative reducing agents in metallurgical processes: gasification of shredder residue material. J Sustain Metall 3:336–349. https://doi.org/10.1007/s40831-016-0096-y
38. Zhang C, Chen S, Miao X, Yuan H (2009) Reduction experiment of iron scale by adding waste plastics. J Environ Sci 21:48–51. https://doi.org/10.1016/S1001-0742(09)60035-8
39. Lahijani P, Zainal ZA, Mohammadi M, Mohamed AR (2015) Conversion of the greenhouse gas CO_2 to the fuel gas CO via the Boudouard reaction: a review. Renew Sustain Energy Rev 41:615–632. https://doi.org/10.1016/j.rser.2014.08.034
40. Roberts DG, Hodge EM, Harris DJ, Stubington JF (2010) Kinetics of char gasification with CO_2 under regime II conditions: effects of temperature, reactant, and total pressure. Energy Fuels 24:5300–5308. https://doi.org/10.1021/ef100980h
41. Strengell D, Avarmaa K, Johto H, Taskinen P (2016) Distribution equilibria and slag chemistry of DON smelting. Can Metall Q 55:234–242. https://doi.org/10.1080/00084433.2016.1169661
42. Sukhomlinov D, Klemettinen L, Avarmaa K, O'Brien H, Taskinen P, Jokilaakso A (2019) Distribution of Ni Co, precious, and platinum group metals in copper making process. Metall Mater Trans B 50B:1752–1765. https://doi.org/10.1007/s11663-019-01576-2
43. Takeda Y, Ishiwata S, Yazawa A (1983) Distribution equilibria of minor elements between liquid copper and calcium ferrite slag. Trans Jpn Inst Met 24:518–528. https://doi.org/10.2320/matertrans1960.24.518

44. Bale CW, Bélisle E, Chartrand P, Decterov SA, Eriksson G et al (2016) CALPHAD: computer coupling of phase diagrams and thermochemistry FactSage thermochemical software and databases, 2010–2016. Calphad 54:35–53. https://doi.org/10.1016/j.calphad.2016.05.002
45. Koskela A, Heikkilä A, Bergna D, Salminen J, Fabritius T (2021) Effects of briquetting and high pyrolysis temperature on hydrolysis lignin char properties and reactivity in Co-CO_2-N_2 conditions. Minerals 11:1–17. https://doi.org/10.3390/min11020187

Authors and Affiliations

Desmond Attah-Kyei[1] · Dmitry Sukhomlinov[1] · Mia Tiljander[2] · Lassi Klemettinen[1] · Pekka Taskinen[1] · Ari Jokilaakso[1] · Daniel Lindberg[1]

✉ Desmond Attah-Kyei
desmond.attah-kyei@aalto.fi

[1] Department of Chemical and Metallurgical Engineering, School of Chemical Engineering, Aalto University, Kemistintie 1, P.O. Box 16100, 00076 Aalto, Finland

[2] Geological Survey of Finland, Vuorimiehentie 2, 02150 Espoo, Finland